Nano Energy 48 (2018) 456–463

Contents lists available at ScienceDirect

Nano Energy

journal homepage: www.elsevier.com/locate/nanoen

Full paper

# Study on friction-electrification coupling in sliding-mode triboelectric nanogenerator

Weiqiang Zhang[a,b], Dongfeng Diao[b,*], Kun Sun[a,b], Xue Fan[b], Pengfei Wang[b,*]

[a] Key Laboratory of Education Ministry for Modern Design and Rotor-Bearing System, School of Mechanical and Engineering, Xi'an Jiaotong University, Xi'an 710049, China

[b] Institute of Nanosurface Science and Engineering (INSE), Guangdong Provincial Key Laboratory of Micro/Nano Optomechatronics Engineering, Shenzhen University, Shenzhen 518060, China

ARTICLE INFO

*Keywords:*
Triboelectric nanogenerator
Sliding-mode
Friction-electrification
Carbon films
Edge and channel effects

ABSTRACT

Triboelectric nanogenerator (TENG) is regarded as a revolutionary technology for harvesting clean and sustainable energy with low cost. Here, sliding-mode TENGs based on both graphene sheets embedded carbon (GSEC) and amorphous carbon (a-C) films were designed and their friction-electrification coupling properties were studied. The GSEC and a-C films were fabricated by electron irradiation assisted physical vapor deposition in an electron cyclotron resonance (ECR) plasma system. A novel testing platform that can simultaneously measure friction force, output voltage and output current was designed and assembled for studying the friction-electrification coupling of sliding-mode TENG. In the case of GSEC and a-C films slid against Polytetrafluoroethylene (PTFE) film, the open-circuit output voltage, the short-circuit output current density, the peak power density and the maximum instantaneous energy conversion efficiency were 13.5 V, 0.35 μA/cm$^2$, 0.63 mW/cm$^2$ and 8.61% for the GSEC film based TENG, and 8.5 V, 0.24 μA/cm$^2$, 0.5 mW/cm$^2$ and 7.71% for the a-C film based TENG, respectively. The results implied that the GSEC film exhibited a higher electric output performance compared with the a-C film. The origin of high electric output performance of the GSEC film based TENG was ascribed to the edge and channel effects of graphene sheets. These findings shed light on the application of carbon films in friction-induced nanoenergy field.

## 1. Introduction

With the rapid development of portable electronics, smart wearable devices and sensor networks, harvesting energy from ambient environment to reduce the use of batteries has attracted worldwide attentions. Researchers have devoted great efforts to find alternative forms of energy such as thermoelectricity [1,2], piezoelectricity [3,4], pyroelectricity [5], biofuels [6] and nanogenerator to power the wearable electronics [7]. Recently, triboelectric nanogenerator (TENG) receives widespread attentions due to its high energy conversion efficiency, high output voltage and low cost [8–12]. In the four fundamental working modes of TENG, sliding-mode TENG is an important one [13], which is triggered by relative sliding between triboelectric layers [14–16]. Especially, some researchers have found that frictional behavior at the contact interface has an influence on the energy conversion efficiency, output current, output voltage and power of TENG [17,18]. However, to the author's knowledge, little research has been devoted to investigate the frictional behavior at the sliding interface of TENG. Moreover, the relationship between frictional behavior and electrification performance is vague. Clarifying the relationship between friction behavior and electrification performance could promote the practical application progress of sliding-mode TENG.

It is well known that sliding-mode TENG requires two triboelectric layers with opposite charges to establish a potential difference. In the aim of achieving the high output voltage, output current and output power, both polymer films and metallic films have been used as the triboelectric layers [19–22]. However, the corrosion of metal in water or humid environment is a common problem for supplying stable nanoenergy, and new materials for harvesting nanoenergy need to be developed. Carbon is environmental friendly and abundant on earth. Graphene is a rapidly rising star material [23], as a two-dimensional "aromatic" monolayer of carbon atoms with sp$^2$ atomic configuration, the graphene exhibits exceptionally physical properties [24–26]. Some studies have demonstrated that graphene can store electric charge for a period of time, which add its suitability for electronics and TENG [17,27–32]. Lately, our group has proposed a new method to fabricate graphene sheets embedded carbon (GSEC) film in electron cyclotron resonance (ECR) plasma with low energy electron irradiation [33]. In the process of depositing GSEC film, excess electrons may be stored in

* Corresponding authors.
*E-mail addresses:* dfdiao@szu.edu.cn (D. Diao), wangpf@szu.edu.cn (P. Wang).

https://doi.org/10.1016/j.nanoen.2018.04.007
Received 9 January 2018; Received in revised form 3 April 2018; Accepted 3 April 2018
Available online 04 April 2018

graphene sheets. This is similar to electron n-type doping in epitaxial graphene [34]. Theoretical calculation and experimental results have demonstrated that the edge-quantum wells of graphene sheets in GSEC film can capture excess electrons from plasma beam [35,36]. Due to under-coordination, the length of C-C bond at edge will contract significantly compared with that at center to lower the total energy. The potential well to the neighbor electrons will be deepened at the edge site with a consequence of localized densification of charge, energy and mass. In the growing process of GSEC film under low energy electron irradiation, excess electrons tend to be captured by the edge-quantum wells of graphene [35]. Based on the above studies it was anticipated that GSEC film has excellent electric property similar to graphene and may be suitable for TENG. Therefore, it was worthwhile to investigate the friction-electrification performances of GSEC film.

In this study, we introduced a novel testing platform to study the friction-electrification performances of GSEC and a-C films slid against PTFE film. The friction coefficients of GSEC and a-C films against PTFE film were measured. Besides, the electric output performance including output voltage and output current at sliding interface were simultaneously measured. Finally, the relationship between friction coefficient and electric output performances was discussed.

## 2. Experimental section

### 2.1. Deposition of carbon films

An electron irradiation assisted physical vapor deposition in ECR plasma processing system was used for fabricating GSEC and a-C films. In the ECR system, 2.45 GHz microwave with a power of 500 W was introduced to the plasma chamber through a rectangular waveguide and a quartz window. Two sets of magnetic coils were arranged around the chamber to achieve a microwave ECR condition (magnetic flux density, 875 G). Mirror confinement electron cyclotron resonance (MCECR) plasma was generated when DC power was supplied to both of the magnetic coils. A cylindric carbon target was located in the middle of the two magnetic coils as solid carbon source for films deposition. The detailed information about the system had been reported in our previous works [36–38]. The GSEC and a-C films with thickness of 100 nm were deposited on p-type Si (100) wafers (resistivity: < 0.0015 Ω cm, thickness: 525 μm) with the size of 2.5 cm × 2.5 cm. The Si wafers were cleaned with ethyl alcohol and deionized water bath successively by ultrasonic wave. Thereafter, the Si wafers were dried naturally and mounted on the sample holder. The background pressure of the vacuum chamber was pumped down to $7 \times 10^{-5}$ Pa, and the working gas of argon was introduced to keep the chamber pressure to be $4 \times 10^{-2}$ Pa. The GSEC film was fabricated under an electron irradiation energy of 50 eV and an irradiation density of 65 mA/cm$^2$. The a-C film was produced under an electron irradiation energy of 5 eV and an irradiation density of 15 mA/cm$^2$.

### 2.2. Nanostructures characterization

The nanostructures of GSEC and a-C films were observed by using a transmission electron microscope (TEM, JEM-3200, JEOL) with electron acceleration voltage of 300 kV. The bonding structures of the GSEC and a-C films were characterized by using laser confocal Raman spectroscopy (LabRAM HR Evolution, Horiba) with a 532 nm laser. The surface morphologies of GSEC and a-C films were measured by using an atomic force microscope (Dimension Edge, Bruker) with a scanning range of 5 μm × 5 μm. The measurements were repeated three times and an average value was obtained.

### 2.3. Fabrication of TENG

Generally, a TENG mainly consists of an up-part and a down-part. In this work, PTFE film was selected as the up triboelectric layer, Si wafer, GSEC and a-C films were selected as the down triboelectric layer. Fig. 1 shows the fabrication processes of GSEC film based TENG. Up-part: a PTFE film with dimensions of 2.5 cm × 2.5 cm × 0.01 cm was cleaned in the ethyl alcohol and deionized water bath successively by ultrasonic wave. Then, a conductive copper tape was attached on one side of the PTFE film as the top electrode. Down-part: firstly, the surface of GSEC film was blown clean. Then, a layer of conductive copper tape was attached on the unpolished surface of Si wafer as the bottom electrode. When the two parts were integrated with a load circuit, a GSEC film based TENG was fabricated. The fabrication processes of a-C film and Si based TENG were identical to that of GSEC film based TENG.

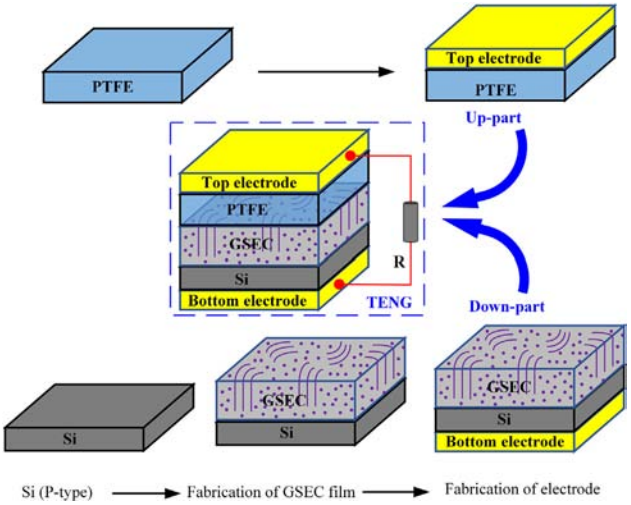


**Fig. 1.** Schematic illustration of the fabrication processes of GSEC film based TENG. A piece of PTFE film was cleaned and a top copper electrode was attached on the upper surface. GSEC film was deposited on the polished surface of Si and a bottom copper electrode was attached on the unpolished surface of Si. When the two parts were integrated with a load circuit, a GSEC film based TENG was fabricated.

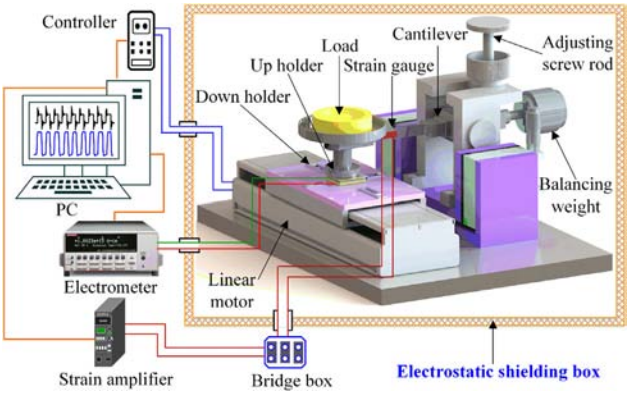


**Fig. 2.** Schematic diagram of the novel testing platform for evaluating friction-electrification coupling of sliding-mode TENG. Two parts of TENG were mounted on the up and down holder. The adjusting screw rod and balancing weight were used to control the contact level status of the two parts. The linear motor drove the down-part reciprocating moving, thus the two parts periodical overlap and separation. The strain gauges were pasted on the cantilever for detecting the friction force. An electrometer was used to measure the output voltage, and a low noise current preamplifier was used to measure the output current. An electrostatic shielding box was designed to improve the anti-interference property and all apparatus were well grounded.

### 2.4. The novel testing platform

A novel testing platform which can simultaneously measure the

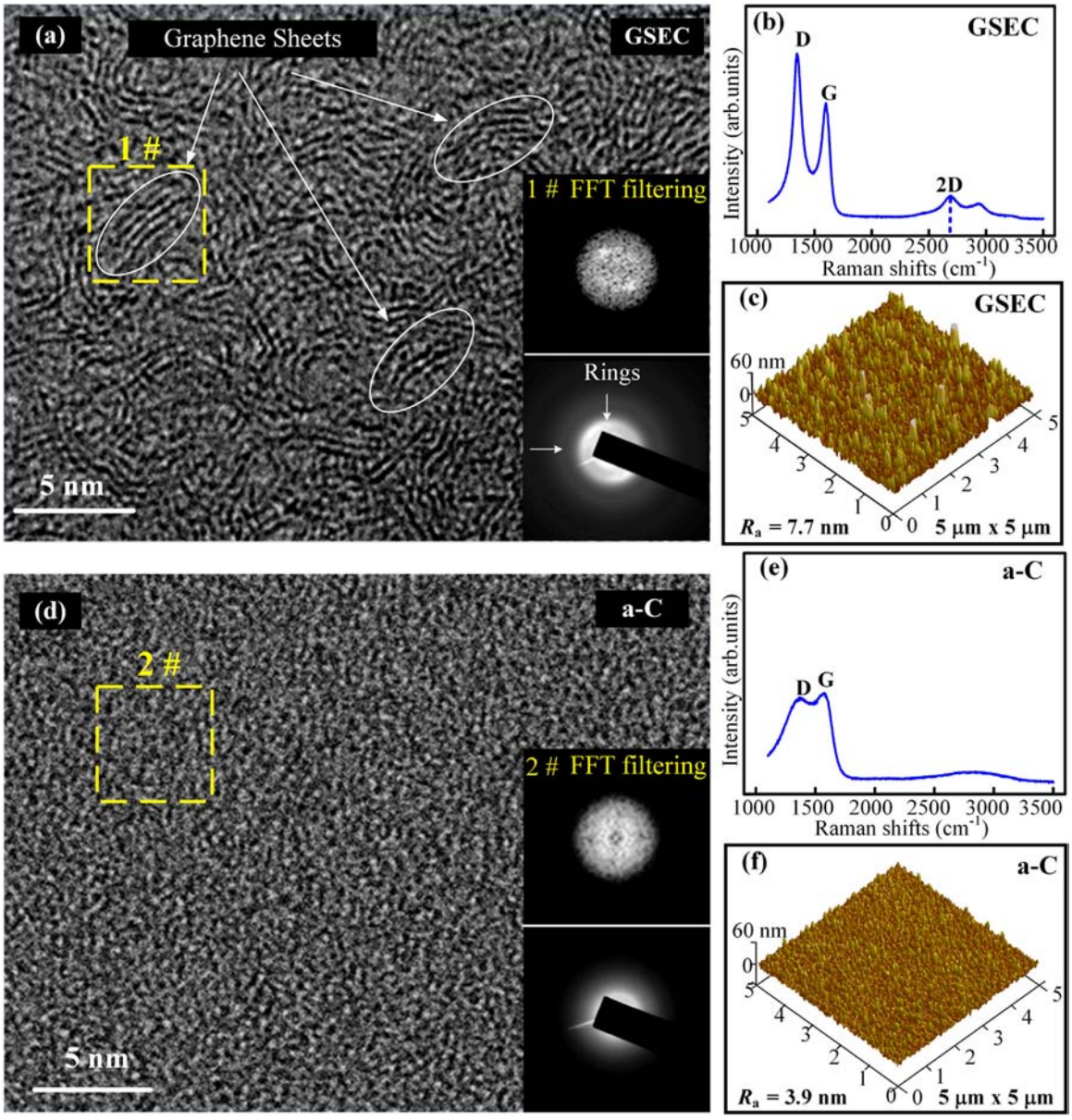


**Fig. 3.** The nanostructures of the GSEC and a-C films. (a) and (d) The plan view TEM images of GSEC and a-C films. It can be clearly observed in (a) that graphene sheets embedded in the amorphous carbon matrix. (b) and (e) The Raman spectra of the GSEC and a-C films. The Raman spectra of GSEC film contained separate D and G bands around 1340 $cm^{-1}$, 1580 $cm^{-1}$. A 2D band was also can be detected around 2700 $cm^{-1}$ in (b). (c) and (f) The surface morphologies of the GSEC and a-C films, and the surface roughness were 7.7 nm and 3.9 nm, respectively.

friction force, output voltage and output current was designed and assembled for studying the friction-electrification coupling performance of TENG. As demonstrated in Fig. 2, the platform mainly consisted of a personal computer (PC), a linear motor, an electrometer (and low noise current preamplifier), a cantilever, two strain gauges, two holders, and an electrostatic shielding box. The up-part was mounted on the up holder and the down-part was fixed on the down holder. The strain gauges were used for detecting the friction force. The output voltage and output current were measured by using an electrometer (6517B, Keithley) and a low noise current preamplifier (SR570, Stanford Research System), respectively. The sampling frequency for the output voltage and output current data was 1000 Hz. An electrostatic shielding box was designed to improve the anti-interference property and all apparatus were well grounded. When the down-part slid, the electric output and friction force were simultaneously measured by the electric apparatus and strain gauges, respectively. In this work, two parts of TENG were not fully separated and the relative displacement was 1 cm, which was two fifth of the length of the TENG. All the experiments were conducted under the condition with the temperature of 25 ± 1.5 °C, and the relative humidity of 65 ± 10%. The normal load was 3 N and the average velocity was 1.92 cm/s. The electric output and friction coefficient of the steady sliding period were used to evaluate the friction-electrification performances.

## 3. Results and discussion

The nanostructures of the two films are shown in Fig. 3. Fig. 3(a) shows the plan view TEM image of GSEC film, and it can be clearly observed that the graphene sheets embedded in the amorphous carbon matrix. The FFT filtering was performed on region 1# and the result was shown in the inset of Fig. 3(a). Two white light spots were obviously found, which implied the existence of graphene nanosheets. The inset picture of Fig. 3(a) also gives the electron diffraction (ED) pattern of the GSEC film, which shows diffraction rings in response to the

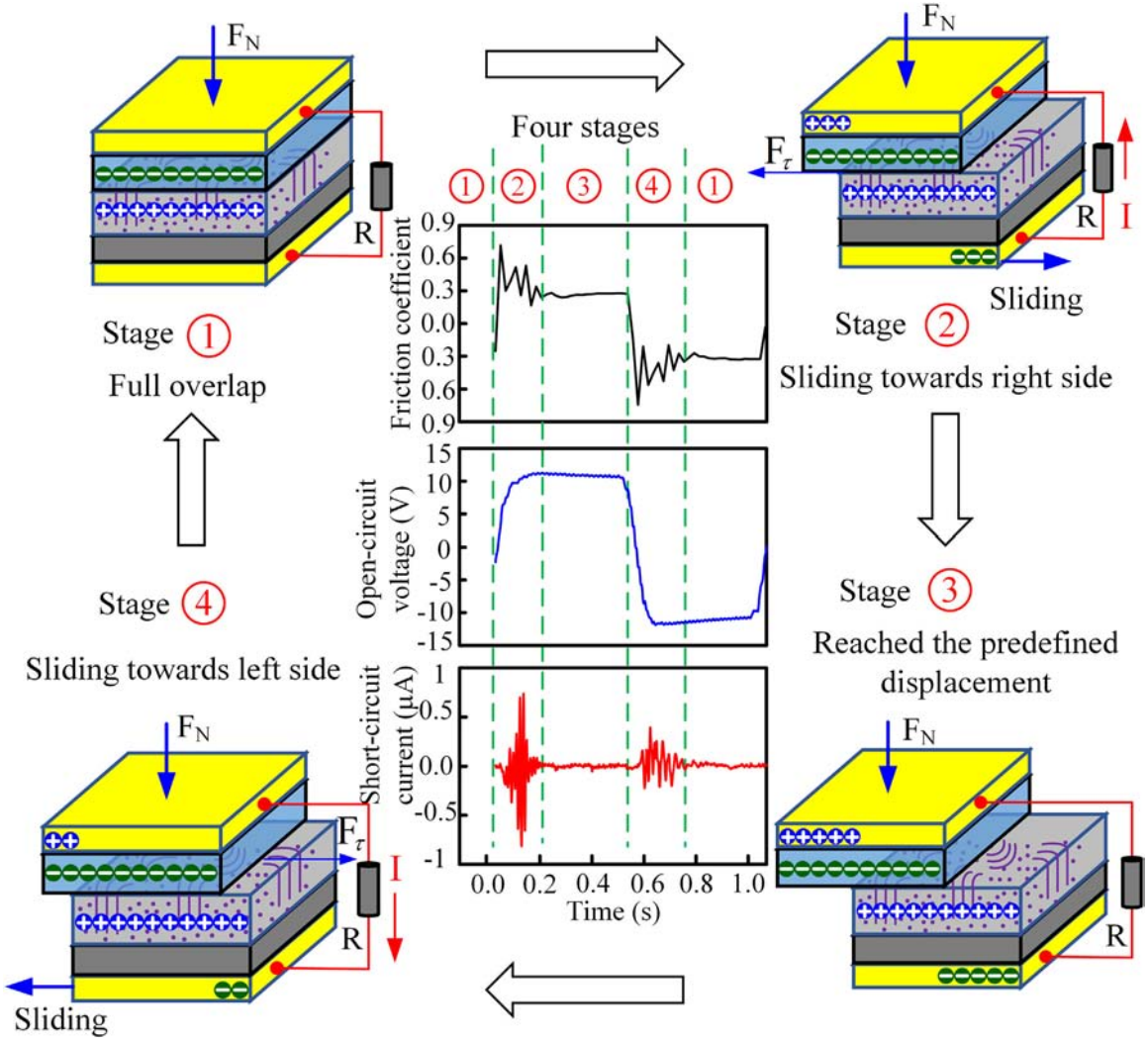


**Fig. 4.** The schematic illustration of the friction-electrification coupling at sliding interface of GSEC film based TENG. At stage 1, GSEC film and PTFE film full overlap and no a friction, output voltage or output current was generated. At stage 2, the GSEC film slid towards right side, and the friction force, output voltage and output current were detected. At stage 3, the GSEC film reached the predefined displacement and kept static for a while. At stage 4, the GSEC film slid towards left side, and the friction force, output voltage and output current were detected.

graphene nanosheets. Fig. 3(d) shows the plan view TEM image of a-C film, and graphene sheets can hardly be found in the film. For the a-C film, the region that performed FFT filtering was marked with 2#, and the result is shown in the inset of Fig. 3(d). There was no white light spot observed in the FFT filtering result. The inset picture of Fig. 3(d) also gives the ED pattern of the a-C film, which shows no diffraction ring. As shown in Fig. 3(b), the Raman spectra of GSEC film contains separate D and G bands around 1340 $cm^{-1}$, 1580 $cm^{-1}$ and the 2D band also can be detected around 2700 $cm^{-1}$. The 2D band suggested the existence of graphene layers since it arises from the two-phonon involved double resonance Raman process, which typically occurs inside the graphene layer [39]. For the a-C film, 2D band was barely seen in the Raman spectra, as shown in Fig. 3(e). Thus, the structural differences between the GSEC and a-C films were well supported by the above results. Fig. 3(c) and (f) show the surface morphologies of the two films, respectively. The mean surface roughness (Ra) of GSEC film was 7.7 nm, and that of a-C film was 3.9 nm, suggesting that the a-C film is smoother than GSEC film. The increasing of surface roughness is induced by the formation of graphene sheets, which was corroborated by the previous reports that the formation of $sp^2$ clusters led to surface roughening [40,41].

GSEC film based TENG was selected to study the friction-electrification coupling at sliding interface. As presented in Fig. 4, the sliding friction process was considered as into four stages. At stage 1, the GSEC film and the PTFE film were full overlap. According to the triboelectric material series [13], the same amount of negative and positive charges was induced on the surfaces of PTFE film and GSEC film. There was no friction force, output voltage or output current. At stage 2, GSEC film slid towards right side. A potential difference was generated between the two electrodes, and electrons flowed from the top electrode to the bottom electrode, thus an output current was generated in the external circuit. Charges were gradually accumulated and the output voltage increased. The friction force can be measured at the same time. At stage 3, GSEC film reached the predefined displacement and kept static state. At this stage, the output voltage kept a constant value and almost no electrons flowed between the two electrodes, and the output current was zero. The friction coefficient at stage 3 was not a real stable friction coefficient and it was induced by the cantilever bending due to the relative displacement between the PTFE film and GSEC film. At stage 4, the GSEC film slid towards left side, GSEC film and PTFE film were gradually full overlapped. The electrons flowed from the bottom electrode to the top electrode, and the direction of the output voltage and output current was reversed. With the reciprocating motion of linear motor, the GSEC film and PTFE film

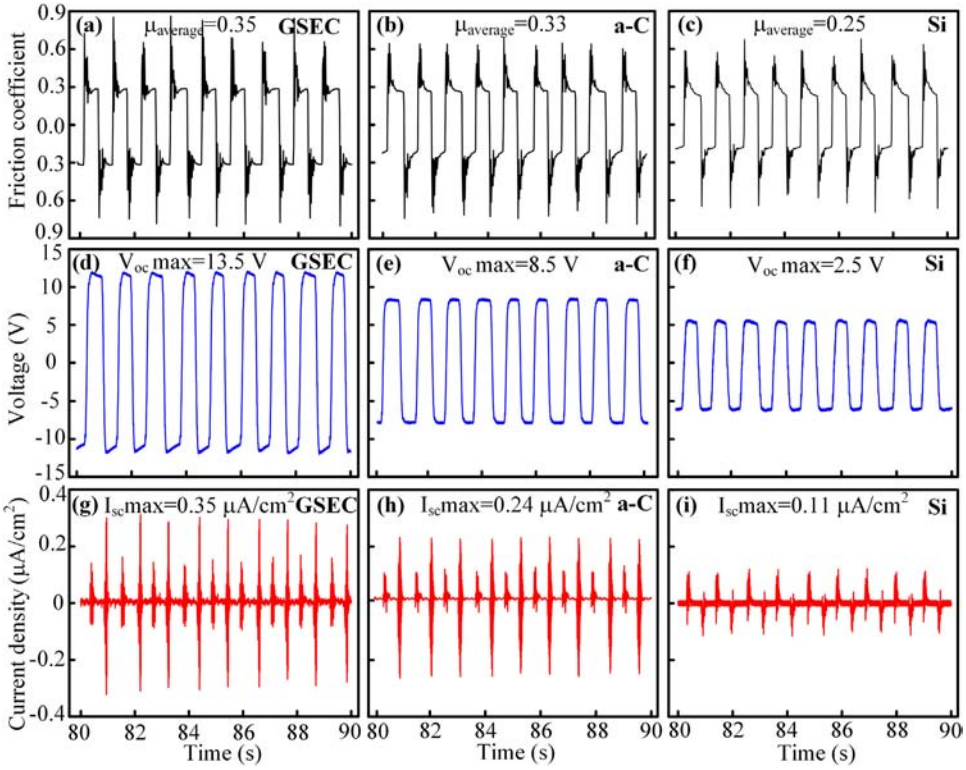


**Fig. 5.** The friction-electrification performances of TENGs. (a-c) The friction curves of the GSEC film, a-C film and Si slid against PTFE film, respectively. The average friction coefficients were calculated using the 100 cycles of friction coefficient data at stages 2 and 4. (d-f) The open-circuit output voltage of the GSEC film, a-C film and Si based TENGs, respectively. (g-i) The short-circuit output current density of the GSEC film, a-C film and Si based TENGs, respectively.

periodical overlapped and separated, and the friction force, output voltage and output current were continuously recorded.

The typical friction coefficient, open-circuit output voltage and short-circuit output current of GSEC film, a-C film and Si against PTFE film were presented in Fig. 5. Fig. 5(a-c) show the detailed friction curves of the GSEC film, a-C film and Si. The average friction coefficient was calculated using the 100 cycles of friction coefficient data at stages 2 and 4. The average friction coefficients of the GSEC film, a-C film and Si were 0.35, 0.33 and 0.25, respectively. It can be found that with the deposition of carbon film on the Si substrate, the friction coefficient increased by about 35%, and the friction coefficient of the GSEC nearly equal to that of a-C films. The output current and power of per unit active area were defined as the output current density and output power density. Fig. 5(d-f) show the maximum open-circuit output voltage of the GSEC film, a-C film and Si based TENGs were 13.5 V, 8.5 V and 5.5 V, respectively. Compared with the Si, the maximum open-circuit output voltage of GSEC and a-C films increased by 145% and 45%. Fig. 5(g-i) show the maximum short-circuit output current density of the GSEC film, a-C film and Si based TENGs were 0.35 μA/cm$^2$, 0.24 μA/cm$^2$ and 0.11 μA/cm$^2$, respectively. Compared with the Si, the maximum short-circuit output current density of the GSEC and a-C films increased by 218% and 118%, respectively.

Similar to the TENGs in other researchers' work [22,42,43], the electric output of the TENGs in our investigation is also a function of the load resistances, with which the output power density can be optimized. Fig. 6(a) shows the resistance-dependent the output voltage and output current density of GSEC film, a-C film and Si based TENGs when the load resistances increased from $1 \times 10^5$ Ω to $1 \times 10^9$ Ω. The output current density dropped with the increasing of load resistances owing to the Ohmic loss, while the output voltage followed a reverse trend. The instantaneous maximum power density can be formulated based on the output current density and the output voltage under different load resistances, whose equation is given by

$$P_{max} = U_{max} \times I_{max} \tag{1}$$

$U_{max}$ and $I_{max}$ are the maximum output voltage and output current under a certain load resistance, respectively. Fig. 6(b) shows the output power density of GSEC film, a-C film and Si based TENGs, and all of them firstly raised and then followed by a drop tendency. The instantaneous maximum output power density of GSEC film based TENG was achieved at a load resistance of about $1 \times 10^8$ Ω, corresponding to a maximum output power density of 0.63 mW/cm$^2$. The instantaneous maximum output power density of a-C film and Si based TENGs were obtained at a load resistance of about $3 \times 10^8$ Ω, corresponding to a maximum output power density of 0.50 mW/cm$^2$ and 0.23 mW/cm$^2$, respectively. Fig. 6(c-e) show the friction force details of the GSEC film, a-C film and Si slid against PTFE film under different load resistances, respectively. It can be found that with the increasing of load resistance, the friction force exhibited a slight increase tendency. These can be explained by the Coulomb force. With the increasing of load resistances, the flow of electrons at the sliding interface was impeded, thus more electrons accumulated and the Coulomb force increased. For evaluating the instantaneous energy conversion efficiency, 10 cycles of output peak power were chosen to calculate the total output electric energy, whose equation is given by

$$E_{output} = \int_0^T U_{max} \times I_{max} dt \tag{2}$$

The input mechanical energy was calculated, whose equation is given by

$$E_{input} = \int_0^S F_\tau ds \tag{3}$$

In Eq. (3), $S$ is the total slid distance of the down-part during 10 cycles and $F_\tau$ is the average friction force. The instantaneous energy conversion efficiency was calculated by the ratio of output electric energy to the input mechanical energy, whose equation is given by

$$\eta = \frac{E_{output}}{E_{input}} = \frac{\int_0^T U_{max} \times I_{max} dt}{\int_0^S F_\tau ds} \times 100\% \tag{4}$$

Fig. 6(f) gives the instantaneous energy conversion efficiency of GSEC, a-C film and Si based TENGs under different load resistances, the

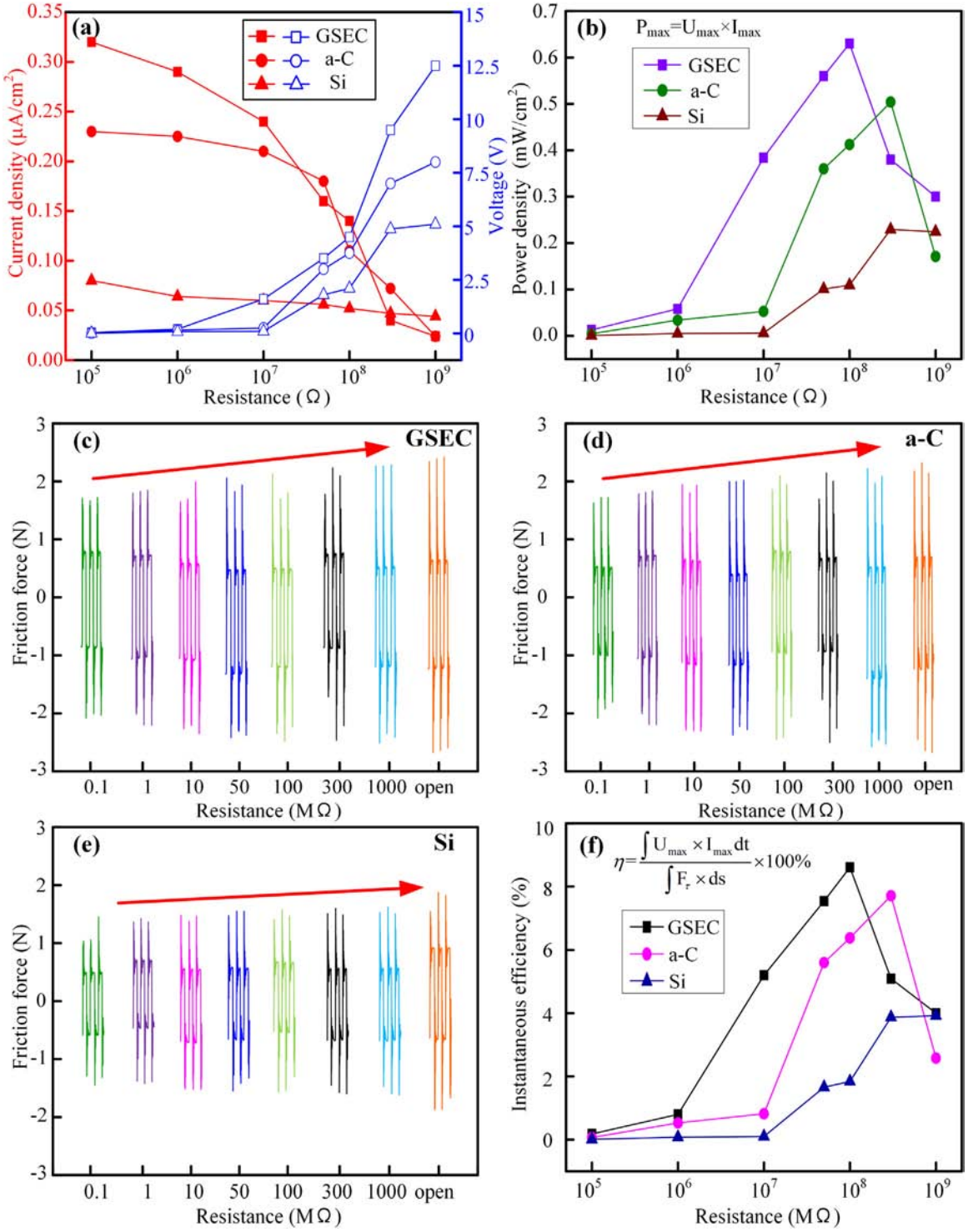


**Fig. 6.** (a) The resistance-dependent output voltage and output current density of GSEC film, a-C film and Si based TENGs under the different load resistances. (b) The maximum output power density of GSEC film, a-C film and Si based TENGs. All of them firstly raised and followed by a drop tendency. (c-e) The friction force of GSEC film, a-C film and Si slid against PTFE film under the different load resistances. (f) The instantaneous energy conversion efficiency of GSEC film, a-C film and Si based TENGs under the different load resistances.

maximum instantaneous energy conversion efficiency of them are 8.61%, 7.71%, 3.92%, with the load resistances of $1 \times 10^8$ Ω, $3 \times 10^8$ Ω and $1 \times 10^9$ Ω, respectively.

Our study showed that the GSEC film slid against PTFE film exhibited the highest friction coefficient, output voltage and output current. The maximum open-circuit output voltage and short-circuit output current density were 13.5 V and 0.35 μA/cm$^2$, which are close to those of Cu foil-grown 1 L graphene-PET TENG [17]. The peak power density and the maximum instantaneous energy conversion efficiency of GSEC film were 0.63 mW/cm$^2$ and 8.61%, respectively. Here, we try to clarify the high friction-electrification performances mechanism of the GSEC film from the views of friction coefficient, edge and channel effects of graphene sheets. It can be seen that the maximum output voltage and output current density are corresponding to the maximum average

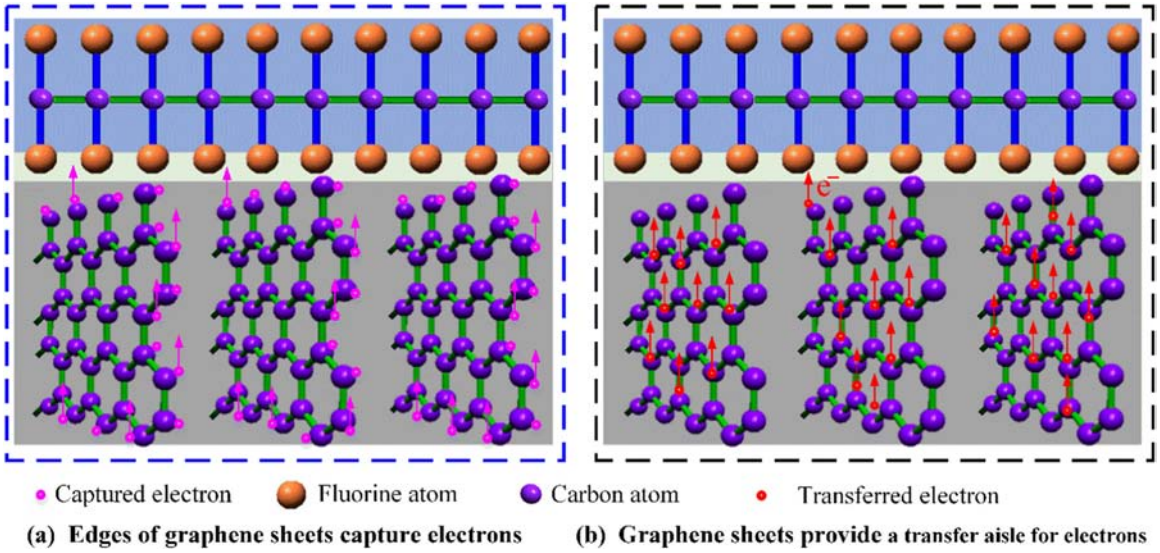


**Fig. 7.** The mechanism of graphene sheets induced high friction-electrification. (a) The edge effect of graphene sheets. Excess electrons were captured by edge-quantum wells of graphene sheets during GSEC film fabrication process. (b) The channel effect of graphene sheets. The graphene sheets embedded in carbon film provides a transfer aisle for electrons and enhanced electron mobility.

friction coefficient. It was suggested that under the identical normal load and working condition, the high friction coefficient may be beneficial to the increase of contact area which leads to high induced charge density on the contact surface of GSEC film and PTFE film, and thus results in the increase of output voltage and output current density.

The friction coefficient of GSEC film and a-C film was nearly the same, the output voltage and output current density of GSEC film was much higher than that of a-C film. Therefore, we proposed that the graphene sheets embedded in pure carbon film play a very important role. On one hand, the graphene sheets can capture electrons due to edge effect during GSEC film fabrication with low energy electron irradiation [35,44]. The excess electrons resulted in the increase of free electrons in GSEC film, as is shown in Fig. 7(a). On the other hand, the graphene sheets provided a transfer aisle for electron migration, which enhanced the electron mobility, as shown in Fig. 7(b). During the sliding friction process, the surface charge states of GSEC film and PTFE film were changed, the combination of edge and channel effects resulted in a higher charge density on the contact surfaces. When the GSEC film based TENG was working, more electrons transferred in the external circuit compared with the a-C film based TENG. The edge and channel effects of graphene sheets contributed to the higher output voltage and output current density of GSEC film based TENG.

## 4. Conclusions

In this work, a novel platform that can simultaneously measure the friction force, output voltage and output current was designed and assembled for evaluating the friction-electrification coupling performances. The output voltage, output current density and friction coefficient of GSEC film, a-C film and Si based TENGs were obtained. The average friction coefficient was 0.35 for GSEC film, 0.33 for a-C film and 0.25 for Si, respectively. Compared with a-C film and Si, GSEC film exhibited the highest open-circuit output voltage, short-circuit output current density, the peak power density and the maximum instantaneous energy conversion efficiency, which were 13.5 V, 0.35 μA/cm$^2$, 0.63 mW/cm$^2$ and 8.61%, respectively. The increase of the friction-electrification was explained in terms of friction coefficient, edge and channel effects of graphene sheets. This study suggested that the high friction coefficient is beneficial for improving the output electric performance of TENG, and the GSEC film exhibits a potential in the application of environmental friendly and high performance TENG.

## Acknowledgements

The authors thank the financial support of National Natural Science Foundation of China (Nos. 51575359 and 51405308), and Shenzhen Fundamental Research Subject-Layout Project (JCYJ20160427105015701). The authors thank Dr. C. Wang for his discussion on the TEM images analysis. The authors thank Dr. C. Wang and Dr. M. Yin for their discussions on the TEM images analysis.

## References

[1] Z.H. Ge, X.Y. Liu, D. Feng, J.Y. Lin, J.Q. He, High-performance thermoelectricity in nanostructured earth-abundant copper sulfides bulk materials, Adv. Energy Mater. 6 (2016) 1600607.
[2] M. Noori, H. Sadeghi, C.J. Lambert, High-performance thermoelectricity in edge-over-edge zinc-porphyrin molecular wires, Nanoscale 9 (2017) 5299–5304.
[3] Z.L. Wang, J. Song, Piezoelectric nanogenerators based on zinc oxide nanowire arrays, Science 312 (2006) 242–246.
[4] K. Park, J.H. Son, G.T. Hwang, C.K. Jeong, J.H. Ryu, M. Koo, I. Choi, S.H. Lee, M. Byun, Z.L. Wang, K.J. Lee, Highly-efficient, flexible piezoelectric PZT thin film nanogenerator on plastic substrates, Adv. Mater. 26 (2014) 2514–2520.
[5] C.R. Bowen, J. Taylor, E. Leboulbar, D. Zabek, A. Chauhan, R. Vaish, Pyroelectric materials and devices for energy harvesting applications, Energy Environ. Sci. 7 (2014) 3836–3856.
[6] Y.J. Zhou, N.A. Buijs, Z.W. Zhu, J.F. Qin, V. Siewers, J. Nielsen, Production of fatty acid-derived oleochemicals and biofuels by synthetic yeast cell factories, Nat. Commun. 7 (2016) 11709.
[7] S.M. Li, J. Wang, W.B. Peng, L. Lin, Y.L. Zi, S.H. Wang, G. Zhang, Z.L. Wang, Sustainable energy source for wearable electronics based on multilayer elastomeric triboelectric nanogenerators, Adv. Energy Mater. 7 (2017) 1602832.
[8] F.R. Fan, Z.Q. Tian, Z.L. Wang, Flexible triboelectric generator, Nano Energy 1 (2012) 328–334.
[9] N.Y. Cui, L. Gu, J.M. Liu, S. Bai, J.W. Qiu, J.C. Fu, X.L. Kou, H. Liu, Y. Qin, Z.L. Wang, High performance sound driven triboelectric nanogenerator for harvesting noise energy, Nano Energy 15 (2015) 321–328.
[10] X. He, Y.L. Zi, H. Yu, S.L. Zhang, J. Wang, W.B. Ding, H.Y. Zou, W. Zhang, C.H. Lu, Z.L. Wang, An ultrathin paper-based self-powered system for portable electronics and wireless human-machine interaction, Nano Energy 39 (2017) 328–336.
[11] L. Zhang, B.B. Zhang, J. Chen, L. Jin, W.L. Deng, J.F. Tang, H.T. Zhang, H. Pan, M.H. Zhu, W.Q. Yang, Z.L. Wang, Lawn structured triboelectric nanogenerators for scavenging sweeping wind energy on rooftops, Adv. Mater. 28 (2016) 1650–1656.
[12] L.M. Zhang, C.B. Han, T. Jiang, T. Zhou, X.H. Li, C. Zhang, Z.L. Wang, Multilayer wavy-structured robust triboelectric nanogenerator fort harvesting water wave energy, Nano Energy 22 (2016) 87–94.
[13] Z.L. Wang, Triboelectric nanogenerators as new energy technology for self-powered systems and as active mechanical and chemical sensors, ACS Nano 7 (2013) 9533–9557.
[14] S.H. Wang, L. Lin, Y.N. Xie, Q.S. Jing, S.M. Niu, Z.L. Wang, Sliding-triboelectric nanogenerators based on in-plane charge-separation mechanism, Nano Lett. 13 (2013) 2226–2233.
[15] G. Zhu, J. Chen, Y. Liu, P. Bai, Y.S. Zhou, Q.S. Jing, C.F. Pan, Z.L. Wang, Linear-

grating triboelectric generator based on sliding electrification, Nano Lett. 13 (2013) 2282–2289.
[16] C. Zhang, T. Zhou, W. Tang, C.B. Han, L.M. Zhang, Z.L. Wang, Rotating-disk-based direct-current triboelectric nanogenerator, Adv. Energy Mater. 4 (2014) 1301798.
[17] S. Kim, M.K. Gupta, K.Y. Lee, A. Sohn, T.Y. Kim, K.S. Shin, D. Kim, S.K. Kim, K.H. Lee, H.J. Shin, D.W. Kim, S.W. Kim, Transparent flexible graphene triboelectric nanogenerators, Adv. Mater. 26 (2014) 3918–3925.
[18] L. Lin, Y.N. Xie, S.M. Niu, S.H. Wang, P.K. Yang, Z.L. Wang, Robust triboelectric nanogenerator based on rolling electrification and electrostatic induction at an instantaneous energy conversion efficiency of ~ 55%, ACS Nano 9 (2015) 922–930.
[19] X.F. Wang, S.M. Niu, F. Yi, Y.J. Yin, C.L. Hao, K.R. Dai, Y. Zhang, Z. You, Z.L. Wang, Harvesting ambient vibration energy over a wide frequency range for self-powered electronics, ACS Nano 11 (2017) 1728–1735.
[20] B.B. Zhang, L. Zhang, W.L. Deng, L. Jin, F.J. Chun, H. Pan, B.N. Gu, H.T. Zhang, Z.K. Lv, W.Q. Yang, Z.L. Wang, Self-powered acceleration sensor based on liquid metal triboelectric nanogenerator for vibration monitoring, ACS Nano 11 (2017) 7440–7446.
[21] W. Xu, L.B. Huang, M.C. Wong, L. Chen, G.X. Bai, J.H. Hao, Environmentally friendly hydrogel-based triboelectric nanogenerators for versatile energy harvesting and self-powered sensors, Adv. Energy Mater. 7 (2017) 1601529.
[22] G. Zhu, Y.S. Zhou, P. Bai, X.S. Meng, Q.S. Jing, J. Chen, Z.L. Wang, A shape-adaptive thin-film-based approach for 50% high-efficiency energy generation through micro-grating sliding electrification, Adv. Mater. 26 (2014) 3788–3796.
[23] A.K. Geim, K.S. Novoselov, The rise of graphene, Nat. Mater. 6 (2007) 183–191.
[24] A.A. Balandin, S. Ghosh, W.Z. Bao, I. Calizo, D. Teweldebrhan, F. Miao, C.N. Lau, Superior thermal conductivity of single-layer graphene, Nano Lett. 8 (2008) 902–907.
[25] V. Singh, D. Joung, L. Zhai, S. Das, S.I. Khondaker, S. Seal, Graphene based materials: past, present and future, Prog. Mater. Sci. 56 (2011) 1178–1271.
[26] A.V. Rozhkov, G. Giavaras, Y.P. Bliokh, V. Freilikher, F. Nori, Electronic properties of mesoscopic graphene structures: charge confinement and control of spin and charge transport, Phys. Rep. 503 (2011) 77–114.
[27] Z. Wang, R.W. Scharstein, Electrostatics of graphene: charge distribution and capacitance, Chem. Phys. Lett. 489 (2010) 229–236.
[28] C.G. Liu, Z.N. Yu, D. Neff, A. Zhamu, B.Z. Jang, Graphene-based supercapacitor with an ultrahigh energy density, Nano Lett. 10 (2010) 4863–4868.
[29] C.G. Hu, L. Song, Z.P. Zhang, N. Chen, Z.H. Feng, L.T. Qu, Tailored graphene systems for unconventional applications in energy conversion and storage devices, Energy Environ. Sci. 8 (2015) 31–54.
[30] E.B. Secor, S. Lim, H. Zhang, C.D. Frisbie, L.F. Francis, M.C. Hersam, Gravure printing of graphene for large-area flexible electronics, Adv. Mater. 26 (2014) 4533–4538.
[31] B.D. Choi, M.Y. Choi, W.M. Choi, H.J. Shin, H.K. Park, J.S. Seo, J.B. Park, S.M. Yoon, S.J. Chae, Y.H. Lee, S.W. Kim, J.Y. Choi, S.Y. Lee, J.M. Kim, Fully rollable transparent nanogenerators based on graphene electrodes, Adv. Mater. 22 (2010) 2187–2192.
[32] X.N. Xia, J. Chen, G.L. Liu, M.S. Javed, X. Wang, C.G. Hu, Aligning graphene sheets in PDMS for improving output performance of triboelectric nanogenerator, Carbon 111 (2017) 569–576.
[33] C. Wang, D.F. Diao, X. Fan, C. Chen, Graphene sheets embedded carbon film prepared by electron irradiation in electron cyclotron resonance plasma, Appl. Phys. Lett. 100 (2012) 231909.
[34] C. Coletti, C. Riedl, D.S. Lee, B. Krauss, L. Patthey, K. von Kiltzing, J.H. Smet, U. Starke, Charge neutrality and band-gap tuning of epitaxial graphene on SiC by molecular doping, Phys. Rev. B 81 (2010) 235401.
[35] X. Zhang, C. Wang, C.Q. Sun, D.F. Diao, Magnetism induced by excess electrons trapped at diamagnetic edge-quantum well in multi-layer graphene, Appl. Phys. Lett. 105 (2014) 042402.
[36] W.C. Chen, X. Zhang, D.F. Diao, Low-energy electron excitation effect on formation of graphene nanocrystallites during carbon film growth process, Appl. Phys. Lett. 111 (2017) 114105.
[37] C. Wang, D.F. Diao, Cross-linked graphene layer embedded carbon Film prepared using electron irradiation in ECR plasma sputtering, Surf. Coat. Technol. 206 (2011) 1899–1904.
[38] P.F. Wang, W.Q. Zhang, D.F. Diao, Low friction of graphene nanocrystallite embedded carbon nitride coatings prepared with MCECR plasma sputtering, Surf. Coat. Technol. 332 (2017) 153–160.
[39] L.M. Malard, M.A. Pimenta, G. Dresselhaus, M.S. Dresselhaus, Raman spectroscopy in graphene, Phys. Rep. 473 (2009) 51–87.
[40] O.V. Penkov, V.E. Pukha, E.N. Zubarev, S.S. Yoo, D.E. Kim, Tribological properties of nanostructured DLC coatings deposited by C 60 ion beam, Tribol. Int. 60 (2013) 127–135.
[41] X.L. Peng, Z.H. Barber, T.W. Clyne, Surface roughness of diamond-like carbon films prepared using various techniques, Surf. Coat. Technol. 138 (2001) 23–32.
[42] I.W. Tcho, W.G. Kim, S.B. Jeon, S.J. Park, B.J. Lee, H.K. Bae, D. Kim, Y.K. Choi, Surface structural analysis of a friction layer for a triboelectric nanogenerator, Nano Energy 42 (2017) 34–42.
[43] X. He, Y.L. Zi, H.Y. Guo, H.W. Zheng, Y. Xi, C.S. Wu, J. Wang, W. Zhang, C.H. Lu, Z.L. Wang, A highly stretchable fiber-based triboelectric nanogenerator for self-powered wearable electronics, Adv. Funct. Mater. 27 (2017) 1604378.
[44] C. Wang, D.F. Diao, Self-magnetism induced large magnetoresistance at room temperature region in graphene nanocrystallited carbon film, Carbon 112 (2017) 162–168.

**Weiqiang Zhang** received his master degree from Lanzhou University of Technology, in 2015, and now he is a Ph.D candidate in School of Mechanical Engineering at Xi'an Jiaotong University under the supervision of Prof. Dongfeng Diao. His research interests are nano-tribology and triboelectric nanogenerator.

**Dongfeng Diao** received his Ph.D. degree in Mechanical Engineering from Tohoku University, Sendai, Japan, 1992. He is currently a distinguished professor and director for Institute of Nanosurface Science and Engineering (INSE) and Electron Microscope Center (EMC) at Shenzhen University, Shenzhen, China. His research interests include nanosurface science and technology, nanotriboelectronics and triboquantum.

**Kun Sun** is a Ph.D. candidate in School of Mechanical Engineering at Xi'an Jiaotong University under the supervision of Prof. Dongfeng Diao. His research is focused on the carbon material and its frictional property. He is interested in understanding the origin of the ultra-low friction.

**Xue Fan** received her Ph.D. degree in Mechanical Engineering from Xi'an Jiaotong University, Xi'an, China, 2012. She is currently a associate researcher with the department of College of Mechatronics and Control Engineering Shenzhen University, China. Her current research interests include nanostructured carbon film fabrication and in-situ nanotribology with TEM.

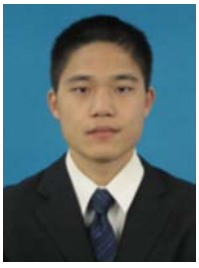

**Pengfei Wang** received his B.S. and M.S. degrees from Xi'an Jiaotong University, Xi'an, China, in 2004 and 2007, respectively, and the Ph.D. degree from Tohoku University, Sendai, Japan, 2011. He is currently a associate researcher with the department of College of Mechatronics and Control Engineering, Shenzhen University, China. His current research is focused on the super-low friction mechanism of carbon film and carbon film based triboelectric nanogenerator.